Journal of Magnetism and Magnetic Materials 343 (2013) 27–31

Contents lists available at SciVerse ScienceDirect

Journal of Magnetism and Magnetic Materials

journal homepage: www.elsevier.com/locate/jmmm

Structural analysis of nanocrystals and their role in the coercivity mechanism of Nd–Fe–Al–Dy bulk amorphous ferromagnets

X.H. Tan [a,*], S.J. Collocott [b], H.W. Liu [c], X.Y. Xiong [d], H. Xu [a]

[a] Laboratory for Microstructures, Shanghai University, Shanghai 200444, PR China
[b] CSIRO Materials Science and Engineering, Lindfield, NSW 2070, Australia
[c] Australian Centre for Microscopy & Microanalysis, The University of Sydney, NSW 2006, Australia
[d] Monash Centre for Electron Microscopy, Monash University, Victoria 3800, Australia

ARTICLE INFO

Article history:
Received 17 September 2012
Received in revised form
22 February 2013
Available online 23 April 2013

Keywords:
Bulk amorphous ferromagnet
Nanocrystal
Coercivity mechanism

ABSTRACT

The magnetic property and microstructure of $Nd_{60-x}Fe_{30}Al_{10}Dy_x$ ($x=0$, 2, 4) bulk ferromagnets have been investigated. At room temperature, each alloy sample shows hard magnetic behavior, and the intrinsic coercivity increases significantly with increasing Dy content. Transmission electron microscopy (TEM) and Atom probe tomography (APT) results show nanocrystals of width 5–20 nm embedded in the Fe-rich amorphous matrix. The coercivity mechanism of the $Nd_{60-x}Fe_{30}Al_{10}Dy_x$ ($x=0$, 2, 4) amorphous alloys is discussed in the context of Gaunt's strong pinning model of domain walls. The crystallographic phases of nanocrystals identified by high-resolution TEM can act as pinning centers. Our findings give further insight into the coercivity mechanism of Nd-based bulk amorphous alloys through a better understanding of the nanostructural environment.

© 2013 Elsevier B.V. All rights reserved.

1. Introduction

Bulk amorphous Nd–Fe–Al alloys were first reported in 1996 [1] and have attracted considerable attention due to their hard magnetic behavior at room temperature, and as a consequence they may be possible candidates for use as permanent magnets. There have been a number of structural investigations of Nd-based bulk amorphous alloys, and a common feature of the microstructure is the presence of nanocrystals, varying in diameter from 1.2 nm to 20 nm, embedded in an amorphous matrix [2–7]. There is continuing debate about the crystallographic phases of nanocrystals. For example, the nanocrystals are believed to be a Nd-rich phase [7–11] or a Nd–Fe phase [12], while other reports suggest that they are Nd–Fe–Al or a δ-phase [2]. Furthermore, there is continuing discussion about the composition of the amorphous matrix, with an Fe-rich amorphous matrix reported by Schneider et al. [7] whilst other studies have found the amorphous matrix to be Nd-rich [2,13–15]. Additionally, there is a debate about the role the microstructure plays in relation to coercivity in these materials. McCallum and his co-workers suggested that the coupling of nanocrystals, with the δ-phase structure ($Nd_6Fe_{13-x}Al_{1+x}$) to the ferromagnetic matrix phase in an "exchange-bias"-type manner conferred high values of coercivity in these materials [2,3]. In contrast, Sun et al. observed rod-like δ-phase crystallites of 50 μm in length in the $Nd_{60}Fe_{30}Al_{10}$ alloy, and argued that the δ-phase was not responsible for the hard magnetic properties [13,16].

Here, a detailed study of the crystallographic structure and chemistry of the nanocrystals is undertaken by transmission electron microscopy (TEM) and atom probe tomography (APT). This work aims to decipher the crystallographic phases present in the nanocrystals; determine the role of Dy, if any, in modifying the nanocrystal crystallographic phases present and gain a better understanding of the composition of the amorphous matrix. On the other hand, our previous work [17] has elucidated that the temperature dependence of the coercivity of the $Nd_{60-x}Fe_{30}Al_{10}Dy_x$ ($x=0$, 2, 4) alloys is in good agreement with Gaunt's model, indicating that the strong pinning model provides a convincing explanation as to the origin of coercivity in these materials. Hence, the other aim of this study is to clarify the role these nanocrystals play in the coercivity mechanism, for example, as to whether they act as pinning centers. It will be helpful to gain further insights into the hard magnetic behavior of these materials from a deeper appreciation of the nanostructural environment.

2. Experimental

Ingots of composition $Nd_{60-x}Fe_{30}Al_{10}Dy_x$ ($x=0$, 2, 4) were prepared by arc melting the mixture of pure elements Nd (99.9%), Fe (99.99%), Al (99.99%) and Dy (99.9%) in an argon atmosphere. The rod samples of 80 mm in length and 3 mm in diameter were

* Corresponding author. Tel.: +86 21 56337032; fax: +86 21 56337887.
E-mail addresses: tanxiaohua123@shu.edu.cn, tanxiaohua123@163.com (X.H. Tan).

0304-8853/$ - see front matter © 2013 Elsevier B.V. All rights reserved.
http://dx.doi.org/10.1016/j.jmmm.2013.04.055

prepared by suction casting of the molten alloy into a water-cooled copper mold. Transmission electron microscopy (TEM) was performed by using a JEOL 2200FS microscope with a field emission electron gun working at 200 kV. An ion beam milling method with Gatan PIPS equipment was employed to prepare the thin specimens of the as-cast alloys for the TEM study. Atom probe tomography (APT) analysis was performed on an Oxford Nano-Science energy compensated atom probe at a temperature of 60 K. Specimens for the APT were prepared by cutting the rod into square bars of dimensions $0.4 \times 0.4 \times 8\ mm^3$ and electropolishing the square bar to a diameter of $\sim 5\ \mu m$ using a solution of 2% $HClO_4$+98% 2-butoxyethanol at 18 V. The final sample was obtained by re-sharpening using an FEI Quanta 3D FEG focused ion beam (FIB) system with an aperture of 500 nm internal diameter and beam current of 0.5 nA.

3. Results

The major hysteresis loops of the $Nd_{60-x}Fe_{30}Al_{10}Dy_x$ ($x=0$, 2, 4) alloys at room temperature are shown in Fig. 1. Each alloy sample shows single phase hard magnetic behavior. The intrinsic coercivity ($\mu_0 H_c^i$) increases, while the saturation magnetization and remanence decrease monotonically with increasing Dy content. It is worth noting that with increasing Dy content, $\mu_0 H_c^i$ increases significantly from 0.3375 T, $x=0$, to 0.5365 T, $x=4$, up 40%. Key magnetic parameters at room temperature are given in Ref. [17].

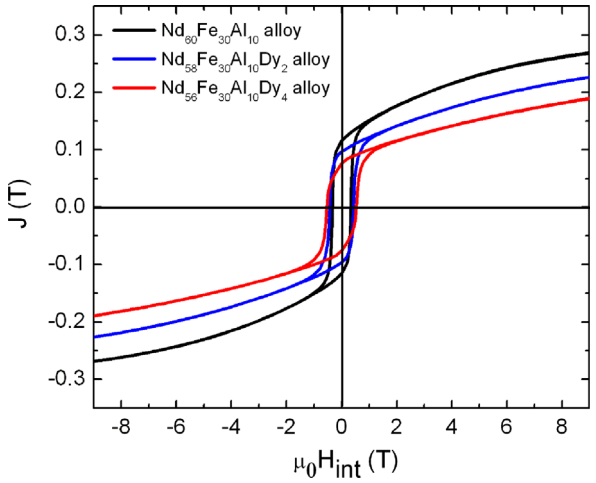

Fig. 1. Hysteresis loops for the $Nd_{60-x}Fe_{30}Al_{10}Dy_x$ ($x=0$, 2, 4) alloys measured at room temperature.

Fig. 2(a) shows the X-ray diffraction results for the $Nd_{60-x}Fe_{30}Al_{10}Dy_x$ ($x=0$, 2, 4) alloys. It is seen that the three alloys have similar XRD curves, with some broad and weak diffraction peaks superimposing on the amorphous bumps, indicating a microstructure composed of nanocrystalline and amorphous phases. There are two positions of the bump, one is at $2\theta=32^\circ$, the other is at $2\theta=60^\circ$. Some diffraction peaks superimpose on the two bumps are identified as a Nd phase. The grain size at about $2\ \theta=60^\circ$ can be calculated by Scherrer Equation [18], and values are given in Table 1. It is seen that the mean grain size of nanocrystals decreases with increasing Dy content. Moreover, the bright-field TEM image of the $Nd_{58}Fe_{30}Al_{10}Dy_2$ alloy (see Fig. 1(b)) shows the nanocrystals are 5–20 nm in size, embedded on the amorphous phase. The selected area diffraction pattern (SADP), shown as an inset in Fig. 2(b), exhibits discontinuous rings, an indicative of fine polycrystallines. In an effort to clarify the crystallographic structure of the nanocrystals, more exhaustive HRTEM investigations were undertaken, and these results are shown in Figs. 3 and 4.

For the $Nd_{60}Fe_{30}Al_{10}$ sample, the majority of nanocrystals are identified as a FCC Nd phase and dHCP Nd phase. For example, Fig. 3(a) and (c) show two nanocrystals, marked as a triangle with a solid line and a rectangle with a solid line, respectively. The corresponding fast Fourier transformation (FFT) images of the selected areas (marked as squares with a solid line) are shown in Fig. 3(b) and (d). They are indexed as the FCC Nd phase and dHCP Nd phase, respectively. For the $Nd_{58}Fe_{30}Al_{10}Dy_2$ sample, both the FCC Nd phase and the dHCP Nd phase are also observed. Furthermore, a Nd_5Fe_{17} phase is found, as shown in Fig. 4(a)–(c). The crystal structure of the Nd_5Fe_{17} phase belongs to the hexagonal space group $P6_3/mcm$ [19]. For the $Nd_{56}Fe_{30}Al_{10}Dy_4$ amorphous alloy, in addition to the FCC Nd phase and the dHCP Nd phase, a δ-phase ($Nd_6Fe_{14-x}Al_x$, $(2<x<5.5)$)

Table 1
The mean grain size of nanocrystals calculated by Sherrer equation [18] for the Nd-based alloys with different Dy content.

Alloys	Bump position (2θ)	
		60°
	Mean grain size (nm)	
$Nd_{60}Fe_{30}Al_{10}$		6
$Nd_{58}Fe_{30}Al_{10}Dy_2$		4
$Nd_{56}Fe_{30}Al_{10}Dy_4$		3

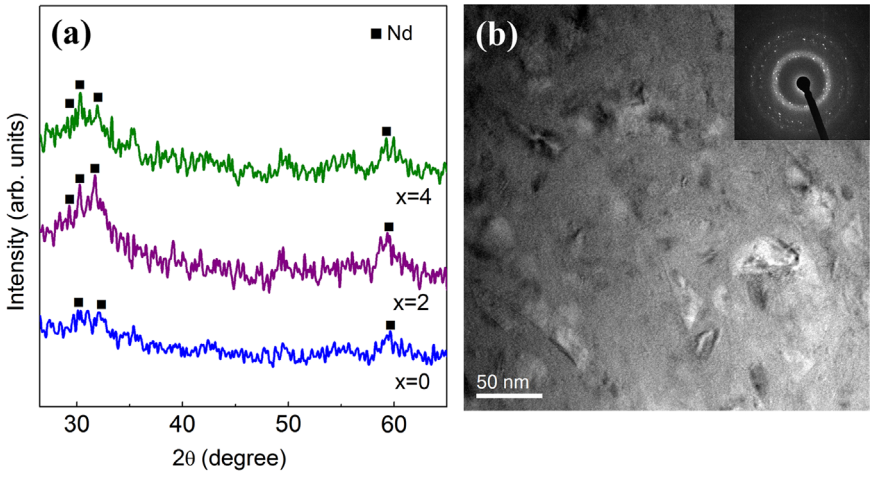

Fig. 2. X-ray diffraction patterns of the $Nd_{60-x}Fe_{30}Al_{10}Dy_x$ ($x=0$, 2, 4) alloys (a) and TEM image for the $Nd_{58}Fe_{30}Al_{10}Dy_2$ alloy (b).

Download English Version:

https://daneshyari.com/en/article/8158067

Download Persian Version:

https://daneshyari.com/article/8158067

Daneshyari.com